

Data-Dependent Hidden Markov Model with Off-Road State Determination and Real-Time Viterbi Algorithm for Lane Determination in Autonomous Vehicles

Mike Stas, Wang Hu, and Jay A. Farrell

arXiv:2505.04763v1 [cs.RO] 7 May 2025

Abstract—Lane determination and lane sequence determination are important components for many Connected and Automated Vehicle (CAV) applications. Lane determination has been solved using Hidden Markov Model (HMM) among other methods. The existing HMM literature for lane sequence determination uses empirical definitions with user-modified parameters to calculate HMM probabilities. The probability definitions in the literature can cause breaks in the HMM due to the inability to directly calculate probabilities of off-road positions, requiring post-processing of data. This paper develops a time-varying HMM using the physical properties of the roadway and vehicle, and the stochastic properties of the sensors. This approach yields emission and transition probability models conditioned on the sensor data without parameter tuning. It also accounts for the probability that the vehicle is not in any roadway lane (e.g., on the shoulder or making a U-turn), which eliminates the need for post-processing to deal with breaks in the HMM processing.

This approach requires adapting the Viterbi algorithm and the HMM to be conditioned on the sensor data, which are then used to generate the most-likely sequence of lanes the vehicle has traveled. The proposed approach achieves an average accuracy of 95.9%. Compared to the existing literature, this provides an average increase of 2.25% by implementing the proposed transition probability and an average increase of 5.1% by implementing both the proposed transition and emission probabilities.

Index Terms—Lane-level map matching, Map matching, Hidden Markov Models (HMM), Viterbi algorithm, Real-time Viterbi algorithm, State estimation

I. INTRODUCTION

ACCURATE vehicle lane determination is essential to Intelligent Transportation Systems (ITS) applications that require knowledge of the vehicle’s current lane for interactions between a vehicle and its neighbors or the roadway infrastructure, for example, Vehicle-to-Everything (V2X) CAV systems, analysis of lane-level vehicle trajectories, traffic patterns, platoon trajectory planning, and intersection management [1], [2]. With the enhanced accuracy of real-time vehicle navigation systems and high-definition maps [3], lane determination is becoming feasible via lane-level map matching [4]–[7]. Lane-level map matching methods differ in how they approach matching estimated vehicle positions to maps [4]–[12].

Map matching methods can be split into three generic approaches. First, point-to-point map matching where a vehicle

This work is intended for submission to the IEEE for possible publication. Copyright may be transferred without notice, after which this version may no longer be accessible.

position is being matched to a node on the map. Second, point-to-curve map matching where a vehicle position is being matched to a lane line (e.g. center line) on the map. Finally, curve-to-curve map matching where a vehicle trajectory is being matched to a lane line (e.g. center line) on the map. The methods described in [4], [5] use a curve-to-curve map matching approach to match vehicle positions to a lane map. The method described in [6] solves the lane determination problem through least squares optimization, while the method described in [7] uses a particle filter. Articles [8]–[13] utilize HMM to solve map matching problems.

Before navigation systems were accurate enough to enable lane-determination, the HMM was studied for road-level map matching in [8], [9], [13]. This work was extended by [10] and [11] to demonstrate lane-level map matching. Their HMM used the vehicle position, velocity, and other measurements to generate emission and transition probabilities for road-level map matching. Once the road was determined, the position error relative to each lane center-line was used for lane-determination.

More recently, [12] used a collection of sensor data such as GPS observations, speed, heading, turn signal, and marker type variables to calculate factors that were multiplied, then normalized to compute an emission probability model. To calculate the transition probability, a maximum depth parameter alongside an added tuning parameter was used, then normalized, to generate the required lane transition probability matrix.

While the existing literature uses the HMM and the Viterbi algorithm to provide working lane-determination methods, there are two main literature gaps that need to be addressed:

- There exists no method of calculating the probability of the vehicle being off-road which causes HMM breaks when the vehicle is not in any lane, for example in an intersection. The literature deals with such breaks through post processing by removing off-road positions from the dataset. Even though post-processing can deal with HMM breaks, the break might be too long where HMM re-initialization is required, thus losing previous vital observation information. Moreover there is no real-time HMM approach that can incorporate off-road positions into the model without re-initializing the HMM at every break.

- HMM transition probability definitions do not condition on observations, instead rely on ad-hoc definitions. While such definitions work, they often depend on fixed probabilities or parameter tuning to improve performance on tested datasets which limits their generalizability as the HMM probabilities will need to be tuned in post processing. This reliance in tuning, which is often overlooked or not thoroughly explained, makes integration into existing CAV systems more challenging.

The paper aims at addressing the gaps by introducing a data-dependent HMM model and a real-time Viterbi algorithm. The contributions of this paper are:

- Presenting an HMM model that directly accounts for the probability of the vehicle being off-road, thus eliminating the possibility of any HMM breaks.
- Developing time-varying and data-dependent emission and transition probability models built on state-space and stochastic models of the vehicle and its navigation systems which are interpreted within the context of lane geometry described by a high-definition roadway map.
- Presenting batch and real-time Viterbi lane determination algorithms that incorporate the proposed data-dependent HMM.
- Proposing a real-time Viterbi lane determination algorithm that has a more informed initialization step by propagating the initial state probability from previous time windows.
- Demonstrating improved performance relative to the existing methods in the literature without any probability parameter tuning or post processing of data to remove off-road observations.

In HMM, the actual lane the vehicle is in at each time is a hidden state that the model tries to infer. Given a sequence of vehicle state vector estimates and its error covariance matrix from the navigation system, the vehicle has some probability of being in each lane at each instant. Then, the sequence of lane transitions can be stochastically modeled and estimated based on the mean and covariance of the vehicle position and velocity, along with the high-definition map, to determine the probability of lane transitions at each time. The HMM has emerged as a powerful tool utilizing the emission and state transition models to determine the most likely sequence of lanes and lane transitions (i.e., the hidden states).

The paper is organized as follows: Section I Introduces lane determination, reviews existing related works, and presents literature gaps to be addressed. Section II states the problem, and reviews and extends HMM definitions and properties to create the data-dependent HMM while adapting it to the lane determination problem. Section III presents the Viterbi algorithm to determine the most likely sequence of lanes, in the context of lane determination where the HMM is time-varying and data-dependent. It also proposes a real-time approach to solving the Viterbi algorithm. Section IV presents the lane model used throughout the paper. Section V-A presents the proposed data-dependent emission probability model. Section V-B presents the proposed data-dependent transition probability model. Section VI presents the required

model modifications for non-parallel lane scenarios. Section VI describes the method of selecting the road segment. Section VII introduces the experimental set-up and procedure, then analyzes the results and performance of different models. Finally, Section VIII concludes the paper and presents future work.

II. LANE DETERMINATION HIDDEN MARKOV MODEL

This section reviews HMMs while adapting their definition [14], [15] to the lane determination problem by introducing data-dependent HMM. The complete HMM is denoted

$$\lambda = (\mathbf{A}_k, \mathbf{B}_k, \pi^+), k = 0, \dots, K. \quad (1)$$

Refer to Table I for symbols used throughout this section.

The symbols \mathbf{A}_k , \mathbf{B}_k , π^+ and K will be defined in the following subsections.

A. Problem Statement

Given a digital map of multi-lane road segments and a sequence of observations O_k for times $t_k = kT$ with $k = 0, \dots, K$, where K is the total number of observations and the sample time T being positive, the challenge is to find the most likely sequence of lanes occupied by the vehicle at each time in this interval. Each observation O_k is an estimate of the mean vehicle position and velocity along with their error covariance matrix. At each time t_k , the road segment is defined by a set of N lanes, indexed by i

$$\mathcal{L}_k = \{L_i\}_{i=0}^N. \quad (2)$$

The lanes L_i for $i \in \{1, \dots, N\}$ are the physical lanes of the road segment. The lane L_0 accounts for the vehicle being off the road (i.e., not in a physical lane). At each time t_k , the vehicle is in one of $L_i \in \mathcal{L}_k$ either in any one of the physical lanes or off the road. Each lane's occupancy will be more or less likely based on the measurement O_k and the lane state at time step t_k . Between times t_k and t_{k+1} some lane transitions will be more or less likely, due to the physical road layout and the state vector of the vehicle. Combining these measurements and state transition probabilities to determine the optimal state sequence is where the HMM and Viterbi algorithm are useful.

Table II summarizes indexing variable definitions used throughout the paper.

| Symbol | Definition |
|--|---|
| λ | Complete Hidden Markov Model |
| L_i | Lane i in the set of available lanes \mathcal{L}_k |
| π_i^-, π_i^+ | Prior and posterior initial state probability of starting in Lane i |
| O_k | Observation at time t_k |
| q_k | The hidden state corresponding to the lane in which the vehicle is located at time t_k |
| \mathbf{X}_k | The vehicle state vector at time t_k |
| $\hat{\mathbf{X}}_k^-, \hat{\mathbf{X}}_k^+$ | Prior and posterior vehicle state estimates at time t_k |
| $\mathbf{C}_{\mathbf{X}_k}^-, \mathbf{C}_{\mathbf{X}_k}^+$ | Prior and posterior covariance matrix at time t_k |
| $b_i(O_k)$ | Emission probability of observing O_k given that the system is in lane L_i |
| a_{ij}^k | The probability of the lane state transitioning from L_i at time t_k to L_j at time t_{k+1} |

TABLE I: Important symbol definitions used throughout Section II

B. Hidden State q_k

The hidden state q_k is the lane in which the vehicle is located at time t_k with $q_k = L_i$ for some $i \in \{0, \dots, N\}$ where $q_k \in \mathcal{L}_k$.

C. Vehicle State-Space Model

The vehicle state vector is defined as¹

$$\mathbf{X}_k = [\mathbf{p}_k \ \mathbf{v}_k]^\top$$

where \mathbf{p}_k and \mathbf{v}_k are the 2D position and velocity. At any time t_k , the vehicle navigation system provides both the prior and posterior state estimates with their error covariance matrices. The state estimates and covariances are defined in Chapter 5 of [16] as

$$\begin{aligned}\hat{\mathbf{X}}_k^+ &= \mathbb{E}\langle \mathbf{X}_k | y_0, \dots, y_k \rangle \\ \mathbf{C}_{\mathbf{X}_k}^+ &= \mathbb{E}\langle (\mathbf{X}_k - \hat{\mathbf{X}}_k^+)(\mathbf{X}_k - \hat{\mathbf{X}}_k^+)^{\top} | y_0, \dots, y_k \rangle \\ \hat{\mathbf{X}}_{k+1}^- &= \mathbb{E}\langle \mathbf{X}_{k+1} | y_0, \dots, y_k \rangle \\ \mathbf{C}_{\mathbf{X}_{k+1}}^- &= \mathbb{E}\langle (\mathbf{X}_{k+1} - \hat{\mathbf{X}}_{k+1}^-)(\mathbf{X}_{k+1} - \hat{\mathbf{X}}_{k+1}^-)^{\top} | y_0, \dots, y_k \rangle\end{aligned}$$

where y_k represent the navigation system sensor measurements at time t_k . The vehicle navigation system could, for example, include a Global Navigation Satellite System (GNSS) [17]–[19], a GNSS aided Inertial Navigation System (INS) [20], [21], or any other localization system used to determine the vehicle state. The methods discussed herein apply regardless of which sensors are used by the navigation system to produce the vehicle state estimates along with their covariance matrix. Note that the state estimate and its covariance matrix will be different at every time step due to noise, changes surrounding environment, and available GNSS constellations. The navigation system is assumed to be able to provide the state estimate and its covariance in Earth-Centered Earth-Fixed (ECEF) (e), intersection North, East, and Down (NED) (g), and lane (ℓ) frame of reference. Pre-superscripts are used to denote the frame-of-reference for points and vectors. For example, ${}^e\mathbf{p}$, ${}^g\mathbf{p}$, and ${}^\ell\mathbf{p}$ indicate the position \mathbf{p} represented in the ECEF, intersection, and lane coordinates, respectively. The frame of reference definitions are reviewed in Appendix A.

The prior state estimate and its error covariance matrix are denoted as

$$\hat{\mathbf{X}}_k^- = [\hat{\mathbf{p}}_k^- \ \hat{\mathbf{v}}_k^-]^\top \text{ and } \mathbf{C}_{\mathbf{X}_k}^- = \begin{bmatrix} \mathbf{C}_{\mathbf{p}_k \mathbf{p}_k}^- & \mathbf{C}_{\mathbf{p}_k \mathbf{v}_k}^- \\ \mathbf{C}_{\mathbf{v}_k \mathbf{p}_k}^- & \mathbf{C}_{\mathbf{v}_k \mathbf{v}_k}^- \end{bmatrix}.$$

The posterior state estimate and its error covariance matrix are denoted as

$$\hat{\mathbf{X}}_k^+ = [\hat{\mathbf{p}}_k^+ \ \hat{\mathbf{v}}_k^+]^\top \text{ and } \mathbf{C}_{\mathbf{X}_k}^+ = \begin{bmatrix} \mathbf{C}_{\mathbf{p}_k \mathbf{p}_k}^+ & \mathbf{C}_{\mathbf{p}_k \mathbf{v}_k}^+ \\ \mathbf{C}_{\mathbf{v}_k \mathbf{p}_k}^+ & \mathbf{C}_{\mathbf{v}_k \mathbf{v}_k}^+ \end{bmatrix}.$$

¹Within the navigation system, the state vector may have additional components, but only position and velocity are used herein.

| Symbol | Definition |
|--------|-------------------------------------|
| k | Time step index |
| i | Lane index at the current time step |
| j | Lane index at the next time step |
| l | Lane index at a previous time step |
| m | Road segment index |

TABLE II: Index definitions used throughout the paper

The posterior state estimates can be propagated through time using the state-space model

$$\begin{aligned}\hat{\mathbf{X}}_{k+1}^- &= \phi \ \hat{\mathbf{X}}_k^+ \\ \mathbf{C}_{\mathbf{X}_{k+1}}^- &= \phi \ \mathbf{C}_{\mathbf{X}_k}^+ \ \phi^\top + \mathbf{Q}_d\end{aligned}$$

where \mathbf{Q}_d is the process noise covariance matrix, and $\phi = \begin{bmatrix} \mathbf{I} & \mathbf{T} \\ \mathbf{0} & \mathbf{I} \end{bmatrix}$ where \mathbf{T} is an identity matrix multiplied by the sampling period Δt such that $\mathbf{T} = \Delta t \ \mathbf{I}$.

D. Observation O_k

The observation is the posterior vehicle state estimate: $O_k = \hat{\mathbf{X}}_k^+$. By the definition of HMM observations in [14], the observation at time t_k (i.e., O_k) depends on the current lane state q_k and is conditionally independent of previous lane states and observations:

$$P(O_k | q_0, \dots, q_k, O_0, \dots, O_{k-1}) = P(O_k | q_k). \quad (3)$$

The vocabulary \mathcal{V} is the set of possible observations at each time step, where each observation $O_k \in \mathcal{V}$. Throughout this article \mathcal{V} is \mathbb{R}^2 . This two dimensional vocabulary corresponds to the roadway surface. The height above the roadway surface is not used within this article, but could be directly incorporated.

The entire sequence of observations is denoted as

$$\mathcal{O} = \{O_k\}_{k=0}^K. \quad (4)$$

To simplify notation during subsequent derivations, the following notation:

$$\mathcal{O}_{k_1}^{k_2} = \{O_{k_1}, \dots, O_{k_2}\} \text{ for } k_2 > k_1, \quad (5)$$

will be used to denote the set of observations between t_{k_1} and t_{k_2} .

E. Emission Probability $b_i(O_k)$

The symbol $b_i(O_k)$ is the emission probability, which represents the probability of the observation O_k given that the system is in lane L_i :

$$b_i(O_k) = P(O_k | q_k = L_i), \quad 0 \leq i \leq N. \quad (6)$$

The emission probability vector $\mathbf{B}_k \in \mathbb{R}^N$ has elements $[\mathbf{B}_k]_i = b_i(O_k)$.

The emission model used herein is discussed in Section V-A.

F. Transition Probability a_{ij}^k

The symbol a_{ij}^k represents the probability of the lane state transitioning from L_i at t_k to L_j at time t_{k+1} :

$$a_{ij}^k = P(q_{k+1} = L_j | q_k = L_i), \quad 0 \leq i, j \leq N.$$

The lane state transition matrix \mathbf{A}_k has elements $[\mathbf{A}_k]_{ij} = a_{ij}^k$. When the road segment changes, the transition probability must take into account new and disappearing lanes; therefore, \mathbf{A}_k may not be a square matrix. The elements of this transition matrix must change with time due to the observations of position and velocity in relation to the high-definition map.

Therefore, the observation O_k must also be taken into account. To achieve this, the transition probability at time t_k , conditioned on observation O_k , is introduced:

$$a_{ij}^k = P(q_{k+1} = L_j | q_k = L_i, O_k), \quad 0 \leq i, j \leq N \quad (7)$$

yielding the data-dependent state transition probability portion of the data-dependent HMM. The introduced transition probability has the following properties:

- A future lane state only depends on the current lane state and observation:

$$\begin{aligned} P(q_{k+1} = L_j | q_k = L_i, q_{k-1}, \dots, q_0, O_0^k) \\ = P(q_{k+1} = L_j | q_k = L_i, O_k). \end{aligned} \quad (8)$$

Conditioning on $q_k = L_i$ relates an assumption about which lane contains the vehicle. Conditioning on O_k provides specific information related to the position and velocity of the vehicle within the lane that affects the probability of each specific lane change.

- Each state transition probability must be non-negative:

$$0 \leq a_{ij}^k \leq 1.$$

- For each i , the probability of transitioning from lane state i to some lane state must sum to 1:

$$\sum_{j=0}^N a_{ij}^k = 1 \quad \forall i. \quad (9)$$

Section III follows the definition in eqn. (7) through the theory, while reviewing the Viterbi algorithm to confirm its feasibility. Section V-B presents the specific lane transition model used herein.

G. Initial State Probability π^-

The symbol π_i^- represents the prior probability, before using any observations, that the system starts in lane i :

$$\pi_i^- = P(q_0 = L_i), \quad 0 \leq i \leq N.$$

The initial state probability vector $\pi^- = [\pi_0^-, \dots, \pi_N^-]$. Before using any initial measurement, it could be reasonable to assume that the system is equally likely to start in any state. If that assumption is invoked, then

$$\pi_i^- = \frac{1}{N+1}. \quad (10)$$

Regardless of the assumptions made, the initial state prior probability vector must have positive components that sum to one

$$\|\pi^-\|_1 = \sum_{i=0}^N \pi_i^- = \sum_{i=0}^N P(q_0 = L_i) = 1.$$

The symbol π_i^+ represents the posterior probability of starting in state i . If no observation of the starting position is available at time $t_k = 0$, the posterior probability is equal to the prior probability (i.e., $\pi_i^+ = \pi_i^-$). If an observation is available at time $t_k = 0$, the posterior initial state likelihood²

²This is a likelihood vector because it only accounts for the one observation O_0 , not all possible observations.

denoted as $\bar{\pi}_i^+$ can be computed using the emission probability $b_i(O_0)$ for observation O_0 :

$$\begin{aligned} \bar{\pi}_i^+ &= P(q_0 = L_i, O_0) \\ &= P(O_0 | q_0 = L_i) P(q_0 = L_i) \\ &= b_i(O_0) \pi_i^-. \end{aligned} \quad (11)$$

The likelihood vector $\bar{\pi}_i^+$ can be converted to a probability vector by normalization:

$$\pi_i^+ = \frac{\bar{\pi}_i^+}{\sum_{i=0}^N \bar{\pi}_i^+}, \quad (12)$$

which satisfies $\|\pi^+\|_1 = 1$.

III. VITERBI HMM LANE DETERMINATION

This section uses the data-dependent HMM definitions presented in Section II to redefine the Viterbi algorithm proposed in [14], [15]. The Viterbi algorithm is then used to solve the lane determination problem by finding the most likely lane sequence of hidden states for a given set of observations. Note that the Viterbi algorithm was originally created for HMM; However, the HMM proposed herein is a data-dependent HMM with a different transition probability definition. Thus, the Viterbi algorithm needs to be redefined to include the data-dependent HMM. Subsection III-A redefines the Viterbi algorithm using the full set of available data \mathcal{O} . Subsection III-B discusses the computational requirements of that approach as the number of measurements increase with time. Subsection III-C presents real-time Viterbi algorithm solutions to the lane determination problem.

Refer to Table III for symbols used throughout this section.

A. The Viterbi Algorithm

Let $\mathcal{Q} = \{q_k\}_{k=0}^K$ represent a lane state sequence. Given a time sequence of observations \mathcal{O} as defined in eqn. (4) and HMM λ as defined in eqn. (1), the Viterbi algorithm determines the hidden state sequence $\mathcal{Q}^* = \{q_k^*\}_{k=0}^K$ that is most likely to have produced \mathcal{O} given λ :

$$\mathcal{Q}^* = \arg \max_{\mathcal{Q}} P(\mathcal{Q}, \mathcal{O} | \lambda). \quad (13)$$

To solve this maximization, it is convenient to introduce the notation:

$$\delta_k^-(i) = \max_{q_0, \dots, q_{k-1}} P(q_0, \dots, q_k = L_i, O_0^{k-1} | \lambda) \quad (14)$$

$$\delta_k^+(i) = \max_{q_0, \dots, q_{k-1}} P(q_0, \dots, q_k = L_i, O_0^k | \lambda), \quad (15)$$

| Symbol | Definition |
|--------------------------------|---|
| \mathcal{Q} | The lane state sequence of the vehicle |
| \mathcal{Q}^* | The optimal lane state sequence of the vehicle given the sequence of observations \mathcal{O} |
| $\delta_k^-(i), \delta_k^+(i)$ | The prior and posterior probability along the most likely sequence of lanes, ending in lane L_i at time t_k |
| $\psi_k(i)$ | back trace variable from lane L_i at time t_k |
| q_k^* | The optimal lane state at time t_k |
| P^* | The joint probability of observations \mathcal{O} and the most probable state sequence \mathcal{Q}^* |

TABLE III: Important symbol definitions used throughout Section III

where $\mathcal{O}_{k_1}^{k_2}$ is defined in eqn. (5). The variables $\delta_k^-(i)$ and $\delta_k^+(i)$ represents the prior and posterior probabilities along the most likely sequence (q_0, \dots, q_{k-1}) , ending in lane L_i at time t_k , accounting for the first $k-1$ and k observations respectively.

Using a direct approach, the time complexity of maximizing eqns. (14) and (15) is $O((N+1)^K)$, where N is the number of physical lanes and K is the number of observations in the sequence. Because the required computational load increases exponentially with K , this approach becomes increasingly infeasible as K increases. Therefore, a more computationally efficient approach is required.

When the probability along the most probable path $\delta_k^+(i)$ for $0 \leq i \leq N$ is known, the probability of the most probable path at time t_{k+1} can be computed recursively using a time propagation and measurement update approach to reduce the number of required calculations:

$$\delta_{k+1}^-(j) = \max_{q_0, \dots, q_k} P(q_0, \dots, q_{k+1} = L_j, \mathcal{O}_0^k | \lambda) \quad (16)$$

$$= \max_{0 \leq i \leq N} \left[\max_{q_0, \dots, q_{k-1}} P(q_0, \dots, q_k = L_i, q_{k+1} = L_j, \mathcal{O}_0^k | \lambda) \right] \quad (17)$$

$$= \max_{0 \leq i \leq N} \left[\max_{q_0, \dots, q_{k-1}} \left[P(q_{k+1} = L_j | q_0, \dots, q_k = L_i, \mathcal{O}_0^k, \lambda) \right. \right. \\ \left. \left. P(q_0, \dots, q_k = L_i, \mathcal{O}_0^k | \lambda) \right] \right] \quad (18)$$

$$= \max_{0 \leq i \leq N} \left[\max_{q_0, \dots, q_{k-1}} \left[P(q_{k+1} = L_j | q_k = L_i, O_k) \right. \right. \\ \left. \left. P(q_0, \dots, q_k = L_i, \mathcal{O}_0^k | \lambda) \right] \right] \quad (19)$$

$$= \max_{0 \leq i \leq N} [a_{ij}^k \delta_k^+(i)]. \quad (20)$$

Note that eqn. (17) is inferred from eqn. (16) by solving for the maximization of q_k first with $\max_{0 \leq i \leq N}$. The transition probability property described in eqn. (8) is then used to simplify eqn. (18) to (19).

The posterior probability $\delta_{k+1}^+(j)$ is calculated as follows

$$\delta_{k+1}^+(j) = \max_{q_0, \dots, q_k} P(q_0, \dots, q_{k+1} = L_j, \mathcal{O}_0^{k+1} | \lambda) \\ = \max_{0 \leq i \leq N} \left[\max_{q_0, \dots, q_{k-1}} P(q_0, \dots, q_k = L_i, q_{k+1} = L_j, \mathcal{O}_0^{k+1} | \lambda) \right].$$

Note that the main difference between the definition of $\delta_{k+1}^-(j)$ and $\delta_{k+1}^+(j)$ is the inclusion of O_{k+1} in the latter. Recall from eqn. (5) that $\mathcal{O}_0^{k+1} = [\mathcal{O}_0^k, O_{k+1}]$, which allows for the following simplification:

$$\delta_{k+1}^+(j) = \\ \max_{0 \leq i \leq N} \left[\max_{q_0, \dots, q_{k-1}} P(q_0, \dots, q_k = L_i, q_{k+1} = L_j, \mathcal{O}_0^k, O_{k+1} | \lambda) \right] \\ = \max_{0 \leq i \leq N} \left[\max_{q_0, \dots, q_{k-1}} \left[P(O_{k+1} | q_0, \dots, q_k = L_i, q_{k+1} = L_j, \mathcal{O}_0^k, \lambda) \right. \right. \\ \left. \left. P(q_0, \dots, q_k = L_i, q_{k+1} = L_j, \mathcal{O}_0^k | \lambda) \right] \right].$$

The observation property described in eqn. (3) along with eqn. (6) and (17) are used to get the following simplification:

$$\delta_{k+1}^+(j) = \max_{0 \leq i \leq N} \left[\max_{q_0, \dots, q_{k-1}} \left[P(O_{k+1} | q_{k+1} = L_j) \right. \right. \\ \left. \left. P(q_0, \dots, q_k = L_i, q_{k+1} = L_j, \mathcal{O}_0^k | \lambda) \right] \right] \\ = \max_{0 \leq i \leq N} \left[\max_{q_0, \dots, q_{k-1}} P(q_0, \dots, q_k = L_i, q_{k+1} = L_j, \mathcal{O}_0^k | \lambda) \right] \\ P(O_{k+1} | q_{k+1} = L_j) \\ = \delta_{k+1}^-(j) b_j(O_{k+1}), \quad (22)$$

The Viterbi algorithm uses the time propagation defined by eqn. (20) and measurement update defined by eqn. (22). This recursive approach reduces the time complexity from the initial $O((N+1)^K)$ to $O(K(N+1)^2)$, making it more viable than the direct approach. Note that adding data dependency to the transition probability does not change the way the Viterbi algorithm is processed or change its time complexity.

To keep track of the states that maximize eqn. (22), the back trace variable $\psi_k(i)$ is introduced. The best sequence of hidden states is generated using the back trace once the final observation has been processed. The Viterbi Algorithm has the following form:

- Initialization: $0 \leq i \leq N$

$$\delta_0^-(i) = \pi_i^- \quad (23)$$

$$\psi_0(i) = 0$$

$$\delta_0^+(i) = \pi_i^- b_i(O_0) \quad (24)$$

- Time propagation and measurement update:

$$0 \leq j \leq N, 0 \leq k < K-1$$

$$\delta_{k+1}^-(j) = \max_{0 \leq i \leq N} [a_{ij}^k \delta_k^+(i)] \quad (25)$$

$$\psi_{k+1}(j) = \arg \max_{0 \leq i \leq N} [a_{ij}^k \delta_k^+(i)]$$

$$\delta_{k+1}^+(j) = \delta_{k+1}^-(j) b_j(O_{k+1}) \quad (26)$$

- Termination:

$$P^* = \max_{0 \leq i \leq N} [\delta_K^+(i)]$$

$$q_K^* = \arg \max_{0 \leq i \leq N} [\delta_K^+(i)]$$

- Optimal state sequence backtracking:

$$\psi_k^* = \psi_{k+1}(q_{k+1}^*), k = K-1, \dots, 0. \quad (27)$$

The initial state probability π_i^- is defined in Section II-G. The emission probability $b_j(O_{k+1})$ is defined in Section II-E. The transition probability a_{ij}^k is defined in Section II-F. The variable P^* is the joint probability of the observations and most probable state sequence, and q_K^* is the start of the back trace. The state sequence $\mathcal{Q}^* = \{q_k^*\}_{k=0}^K$ is the optimal state sequence given the sequence of observations \mathcal{O} .

B. Viterbi Lane Determination Discussion

Fig. 1 shows a visual representation of the Viterbi lane determination algorithm applied to a two-lane road using three observations with time increasing from left to right. Each circle represents one lane from set \mathcal{L}_k , which contains the possible values of the hidden state q_k . The squares represent the observation O_k . The hexagons represent the initial state probability π_i^- . The dotted blue arrows represent a multiplication of the variable at the start of the arrow and the variable on the arrow, resulting in the variable at the end of the arrow.

Fig. 1a corresponds to eqns. (23)-(24) in the initialization step. Fig. 1b corresponds to eqns. (25)-(26) in the time propagation and measurement update step. Each of these subfigure illustrates how the available variables at the start of the computation (left side) and the observations (bottom) are used to calculate the results shown on the right.

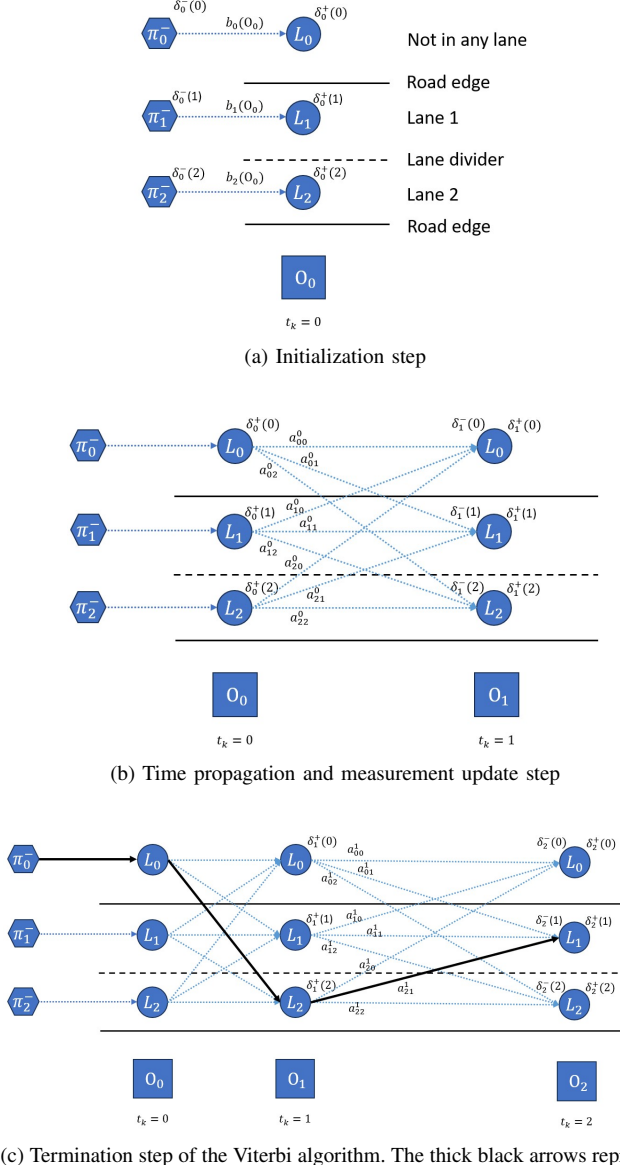


Fig. 1c shows the termination step with $\delta_2^+(1)$ maximizing ψ_2^* . The optimal state sequence of the example is $\mathcal{Q}^* = \{q_0^* = L_0, q_1^* = L_2, q_2^* = L_1\}$. The physical interpretation of the example is as follows: At time $t_k = 0$, the vehicle was off the road. Then at time $t_k = 1$, the vehicle merged into lane L_2 then did a lane change ending in lane L_1 at time $t_k = 2$. Note that L_0 does not have a specific off-lane position, so it could be displayed on either side of the road.

Each $\delta_k^+(j)$ is the probability of ending at state j by the most likely path, based on all observations up to and including time t_k . For each j , its most likely path is distinct. Therefore, the vector of probabilities denoted as δ_k^+ is neither a probability vector or a likelihood vector. The same is true for δ_k^- . Neither $\|\delta_k^+\|_1$ nor $\|\delta_k^-\|_1$ should be expected to equal

one. In fact, as N increases, their 1-norms decrease. At any time the designer chooses, for example to avoid numeric error due to machine precision, δ_k^+ can be normalized such that its 1-norm is equal to one (e.g., see eqn. (12)). The optimal state sequence defined by the maximization in eqn. (13) is unaffected by this normalization.

C. Real-time Viterbi Algorithm

One approach to implement a real-time algorithm that has fixed computational requirements at each time epoch is to use the Viterbi-based approach of the previous section (as summarized in eqns. (23)-(27)) modified as follows. For $0 \leq k \leq n$, the method of Subsection III-A is used with measurements \mathcal{O}_0^n . For $k > n$, the sliding window of the most recent $(n+1)$ measurements \mathcal{O}_{k-n}^k is used. Initialization of this approach for each $k > n$ requires determination of the prior probabilities of each lane at time $(k-n)$ (i.e., $\delta_{k-n}^-(j)$). Two different initialization approaches are as follows.

The first initialization approach uses eqn. (10) to calculate the initial state probability without any prior information:

$$\delta_{k-n}^-(j) = \pi_j^- \text{ and } \delta_{k-n}^+(j) = \pi_j^- b_j(O_{k-n}). \quad (28)$$

The second approach calculates a more informed initial state probability for the current window by propagating the initial state probability from the previous time window. At time step t_k , the prior state probability of time step t_{k-n} is defined as

$$\begin{aligned} \pi_{k-n}^-(j) &\triangleq P(\mathcal{O}_0^{k-n-1}, q_{k-n} = L_j) \\ &= \sum_{i=0}^N P(\mathcal{O}_0^{k-n-1}, q_{k-n-1} = L_i, q_{k-n} = L_j) \\ &= \sum_{i=0}^N P(q_{k-n} = L_j | \mathcal{O}_0^{k-n-1}, q_{k-n-1} = L_i) \\ &\quad P(\mathcal{O}_0^{k-n-1}, q_{k-n-1} = L_i) \end{aligned}$$

$$\begin{aligned} &= \sum_{i=0}^N P(q_{k-n} = L_j | q_{k-n-1} = L_i, O_{k-n-1}) \\ &\quad P(\mathcal{O}_0^{k-n-1}, q_{k-n-1} = L_i) \end{aligned} \quad (29)$$

$$= \sum_{i=0}^N a_{ij}^{k-n-1} P(\mathcal{O}_0^{k-n-1}, q_{k-n-1} = L_i). \quad (30)$$

The posterior state likelihood of time step t_{k-n} is defined as

$$\bar{\pi}_{k-n}^+(j) \triangleq P(\mathcal{O}_0^{k-n}, q_{k-n} = L_j).$$

Therefore, $P(\mathcal{O}_0^{k-n-1}, q_{k-n-1} = L_i)$ in eqn. (30) is equivalent to $\bar{\pi}_{k-n-1}^+(i)$. The fact that $\mathcal{O}_0^{k-n} = [\mathcal{O}_0^{k-n-1}, O_{k-n}]$ allows the following simplification:

$$\begin{aligned} \bar{\pi}_{k-n}^+(j) &= \sum_{i=0}^N P(\mathcal{O}_0^{k-n}, q_{k-n-1} = L_i, q_{k-n} = L_j) \\ &= \sum_{i=0}^N P(O_{k-n} | \mathcal{O}_0^{k-n-1}, q_{k-n-1} = L_i, q_{k-n} = L_j) \\ &\quad P(\mathcal{O}_0^{k-n-1}, q_{k-n-1} = L_i, q_{k-n} = L_j). \end{aligned}$$

The properties of eqns. (3) and (8) allow for the following simplification:

$$\begin{aligned}
\bar{\pi}_{k-n}^+(j) &= \sum_{i=0}^N P(O_{k-n}|q_{k-n} = L_j) \\
&\quad P(O_0^{k-n-1}, q_{k-n-1} = L_i, q_{k-n} = L_j) \\
&= \sum_{i=0}^N P(O_{k-n}|q_{k-n} = L_j) P(O_0^{k-n-1}, q_{k-n-1} = L_i) \\
&\quad P(q_{k-n} = L_j|O_0^{k-n-1}, q_{k-n-1} = L_i) \\
&= P(O_{k-n}|q_{k-n} = L_j) \sum_{i=0}^N P(O_0^{k-n-1}, q_{k-n-1} = L_i) \\
&\quad P(q_{k-n} = L_j|q_{k-n-1} = L_i, O_{k-n-1}). \tag{31}
\end{aligned}$$

Substituting eqns. (6) and (29) into (31) yields

$$\bar{\pi}_{k-n}^+(j) = \left[\sum_{i=0}^N a_{ij}^{k-n-1} \pi_{k-n-1}^+(i) \right] b_j(O_{k-n}).$$

The term in square brackets is the time propagation of the posterior initial likelihood from the previous time window to the start of the current time window. The multiplication by $b_j(O_{k-n})$ computes the posterior initial likelihood of each state for the current time window. Thus, the second initialization approach initializes HMM as

$$\delta_{k-n}^-(j) = \pi_{k-n}^-(j) \text{ and } \delta_{k-n}^+(j) = \bar{\pi}_{k-n}^+(j). \tag{32}$$

IV. LANE MODEL

To utilize the Viterbi algorithm for lane determination, a lane model is required. For the model used herein, each road is decomposed longitudinally into road segments, each segment having a constant number of lanes, as described in eqn. (2). Because the navigation system is accurate enough to enable lane determination (horizontal positional error $< 5m$), it is assumed that the vehicle has already determined which road it is on.

Each lane L_i can be defined by two lane edge curves³. Each curve is defined as a sequence of line segments connecting $M \geq 2$ points:

$$L_i = \begin{bmatrix} {}^g\mathbf{p}_{(u,m)}^i \\ {}^g\mathbf{p}_{(v,m)}^i \end{bmatrix}, \text{ for } m = 1, \dots, M. \tag{33}$$

The symbol ${}^g\mathbf{p}_{(u,m)}^i$ denotes the i -th intersection frame point in a sequence of connected points defining the left lane edge in the direction of traffic flow of the i -th lane. The points ${}^g\mathbf{p}_{(v,m)}^i$ are a sequence of connected points defining the right edge of the lane in the direction of traffic flow of the i -th lane.

Fig. 2 shows the ellipsoidal probability contours for the position estimate $\hat{\mathbf{p}}_k$ relative the m -th segment of lane L_i . Lane frame for segment m of L_i is defined with origin ${}^g\mathbf{p}_{(v,m)}^i$ and axis directions \mathbf{f} and \mathbf{s} . The vector from ${}^g\mathbf{p}_{(v,m)}^i$ to ${}^g\mathbf{p}_{(v,m+1)}^i$ defines the \mathbf{s} -axis, which is the expected direction of travel for L_i . The \mathbf{f} -axis is orthogonal to \mathbf{s} -axis and lies in the plane

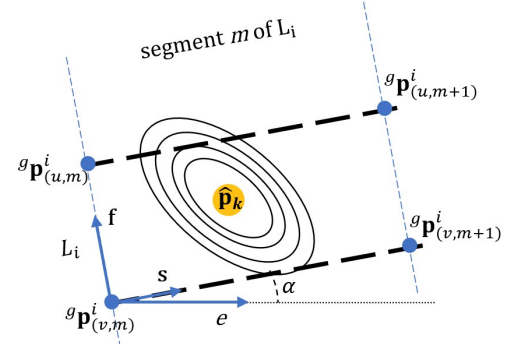


Fig. 2: Lane reference frame: road segment m of lane L_i has a reference frame with origin at ${}^g\mathbf{p}_{(v,m)}^i$ and axis \mathbf{f} and \mathbf{s} . The symbol $\hat{\mathbf{p}}_k$ is the estimated vehicle position at time t_k . The intersection frame e -axis points in the east direction.

of the road surface, defined positively when pointing towards the left edge of the lane. The third dimension of the lane frame is marginalized out as it does not affect the vehicle's position within a lane. In cases where the vertical position of the vehicle is important (e.g., while driving on an overpass), it is assumed that the vertical position is accurate enough to determine the layer of lanes on which the vehicle is traveling.

The pre-superscript (ℓ) is used to denote a position vector represented in lane frame. The pre-subscript (i) will be used to denote the index of lane L_i . For example, ${}^{\ell}\hat{\mathbf{p}}_k^+$ denotes the posterior position estimate $\hat{\mathbf{p}}_k^+$ represented in lane frame of lane L_i .

V. HMM PROBABILITY MODELS

A. Lane Emission Probability Model

This section discusses the method to compute the emission probability at time $t_k = kT$ using O_k for the set of lanes \mathcal{L}_k , defined in Section II-E.

The observation used is $O_k = {}^{\ell}\hat{\mathbf{p}}_k^+$ with its error covariance matrix ${}^{\ell}\mathbf{C}_{\mathbf{p}_k}^+$. The symbol ${}^{\ell}\mathbf{p}_k$ represents the true, but unknown position of the vehicle. By its definition in eqn. (6), the emission probability

$$\begin{aligned}
b_i(O_k) &= P(O_k|q_k = L_i) \\
&= \frac{P(q_k = L_i|O_k) P(O_k)}{P(q_k = L_i)}. \tag{34}
\end{aligned}$$

The subsections that follow will show how to compute $P(q_k = L_i|O_k)$ and $P(q_k = L_i)$. The factor $P(O_k)$ is unknown, but is identical for all $i \in 0, \dots, N$.

Noting the fact that the vehicle has to be either in a lane or off the road, it must be the case that

$$\|\mathbf{B}_k\|_1 = \sum_{i=0}^N b_i(O_k) = 1. \tag{35}$$

Therefore, after computing $P(q_k = L_i|O_k)$ and $P(q_k = L_i)$ the quantity

$$\bar{b}_i(O_k) = \frac{P(q_k = L_i|O_k)}{P(q_k = L_i)} \tag{36}$$

³When the roadway model is defined by lane center-lines as in the SAE J2735 standard, lane edge curves can be computed from the lane width and center-lines.

can be computed and the emission probability elements can be normalized

$$b_i(O_k) = \frac{\bar{b}_i(O_k)}{\sum_{i=0}^N \bar{b}_i(O_k)} \quad (37)$$

to eliminate the unknown $P(O_k)$.

1) *Computation of $P(q_k = L_i | O_k)$* : The factor $P(q_k = L_i | O_k)$ represents the probability that the vehicle is in L_i given the observation O_k . This probability is calculated by integrating the vehicle position probability density over the i -th lane.

The vehicle position probability density conditioned on O_k and represented in the L_i frame is

$$P(\ell_i \mathbf{p}_k | \ell_i \hat{\mathbf{p}}_k^+) = \mathbf{A}_{\mathbf{p}_k} \exp \left(-\frac{1}{2} (\ell_i \mathbf{p}_k - \ell_i \hat{\mathbf{p}}_k^+)^T [\ell_i \mathbf{C}_{\mathbf{p}_k}^+]^{-1} (\ell_i \mathbf{p}_k - \ell_i \hat{\mathbf{p}}_k^+) \right)$$

with $\mathbf{A}_{\mathbf{p}_k} = \frac{1}{2\pi |\ell_i \mathbf{C}_{\mathbf{p}_k}^+|^{1/2}}$. Then, the probability $P(q_k = L_i | O_k)$ is calculated as

$$P(q_k = L_i | O_k) = P(\ell_i \mathbf{p}_k \in L_i | \ell_i \hat{\mathbf{p}}_k^+) = \int_{L_i} P(\ell_i \mathbf{p}_k | \ell_i \hat{\mathbf{p}}_k^+) d\ell_i \mathbf{p}_k.$$

In lane-frame, $\ell_i \mathbf{p}_k$ has coordinates $[s, f]^\top$

$$P(\ell_i \mathbf{p}_k \in L_i | \ell_i \hat{\mathbf{p}}_k^+) = \int_{f \in L_i} \left(\int_{s_0}^{s_e} P((s, f) | \ell_i \hat{\mathbf{p}}_k^+) ds \right) df \quad (38)$$

where s_0 and s_e are the start and end points of the road segment along the s -axis.

The approximation

$$\int_{s_0}^{s_e} P((s, f) | \ell_i \hat{\mathbf{p}}_k^+) ds \approx \int_{-\infty}^{\infty} P((s, f) | \ell_i \hat{\mathbf{p}}_k^+) ds \quad (39)$$

holds for straight lanes (and lanes where the radius of curvature is much larger than the position uncertainty) since it is assumed that $(s_e - s_0) \gg \sigma_s$, where σ_s represents the position uncertainty along the s -axis. The integral $\int_{-\infty}^{\infty} P((s, f) | \ell_i \hat{\mathbf{p}}_k^+) ds$ has the closed form solution

$$\int_{-\infty}^{\infty} P((s, f) | \ell_i \hat{\mathbf{p}}_k^+) ds = A_f \exp \left(-\frac{1}{2} \left(\frac{f - \hat{f}_k^+}{\sigma_{\hat{f}_k^+}} \right)^2 \right), \quad (40)$$

where $A_f = \left(\frac{1}{2\pi \sigma_{\hat{f}_k^+}^2} \right)^{-1/2}$ and the coordinates of $\ell_i \hat{\mathbf{p}}_k^+$ in lane L_i are defined to be $[\hat{s}_k^+, \hat{f}_k^+]^\top$. Substituting eqn. (40) into eqn. (38) yields

$$P(\ell_i \mathbf{p}_k \in L_i | \ell_i \hat{\mathbf{p}}_k^+) = \int_0^{w_i} A_f \exp \left(-\frac{1}{2} \left(\frac{f - \hat{f}_k^+}{\sigma_{\hat{f}_k^+}} \right)^2 \right) df \quad (41)$$

$$= \Phi_f \left(\frac{w_i - \hat{f}_k^+}{\sigma_{\hat{f}_k^+}} \right) - \Phi_f \left(\frac{-\hat{f}_k^+}{\sigma_{\hat{f}_k^+}} \right), \quad (42)$$

where w_i is the lane width, and $\Phi_f()$ is the Cumulative Distribution Function (CDF) of a standard normal random variable.

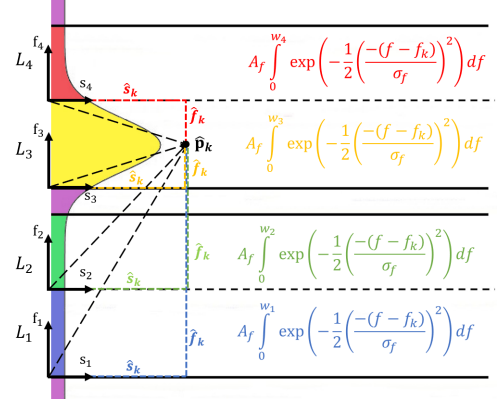


Fig. 3: Illustration of the integral calculations in eqn. (42) or (45) for each lane for position estimate $\hat{\mathbf{p}}_k$. Note that the distribution in the figure was offset to the left from the point $\hat{\mathbf{p}}_k$ to clearly show each colored area along with the formulas.

2) *Computation of $P(q_k = L_i)$* : The factor $P(q_k = L_i)$ represents the probability of being in lane L_i at time t_k before using observation O_k . Thus, the probability can be calculated using the prior estimate $\hat{\mathbf{p}}_k^-$ as

$$\begin{aligned} P(q_k = L_i) &= P(\ell_i \mathbf{p}_k \in L_i | \ell_i \hat{\mathbf{p}}_k^-) \\ &= \int_{L_i} P(\ell_i \mathbf{p}_k | \ell_i \hat{\mathbf{p}}_k^-) d\ell_i \mathbf{p}_k \\ &= \int_{f \in L_i} \left(\int_{s_0}^{s_e} P((s, f) | \ell_i \hat{\mathbf{p}}_k^-) ds \right) df. \end{aligned} \quad (43)$$

The integral in eqn. (43) is calculated similarly to eqn. (38). Using the approximation of eqn. (39), the integral $\int_{-\infty}^{\infty} P((s, f) | \ell_i \hat{\mathbf{p}}_k^-) ds$ will have the closed form solution

$$\int_{-\infty}^{\infty} P((s, f) | \ell_i \hat{\mathbf{p}}_k^-) ds = A_f \exp \left(-\frac{1}{2} \left(\frac{f - \hat{f}_k^-}{\sigma_{\hat{f}_k^-}} \right)^2 \right). \quad (44)$$

Then, $P(\ell_i \mathbf{p}_k \in L_i | \ell_i \hat{\mathbf{p}}_k^-)$ is calculated as

$$\begin{aligned} P(\ell_i \mathbf{p}_k \in L_i | \ell_i \hat{\mathbf{p}}_k^-) &= \int_0^{w_i} A_f \exp \left(-\frac{1}{2} \left(\frac{f - \hat{f}_k^-}{\sigma_{\hat{f}_k^-}} \right)^2 \right) df \\ &= \Phi_f \left(\frac{w_i - \hat{f}_k^-}{\sigma_{\hat{f}_k^-}} \right) - \Phi_f \left(\frac{-\hat{f}_k^-}{\sigma_{\hat{f}_k^-}} \right). \end{aligned} \quad (45)$$

Since $\sum_{i=0}^N P(q_k = L_i | \ell_i \hat{\mathbf{p}}_k^+) = 1$ when conditioned on either $\ell_i \hat{\mathbf{p}}_k^-$ or $\ell_i \hat{\mathbf{p}}_k^+$, the probability of the vehicle being in lane L_0 , interpreted as not in any lane, can be calculated indirectly

$$\begin{aligned} \frac{P(q_k = L_0 | O_k)}{P(q_k = L_0)} &= \frac{P(q_k = L_0 | \ell_i \hat{\mathbf{p}}_k^+)}{P(q_k = L_0 | \ell_i \hat{\mathbf{p}}_k^-)} \\ &= \frac{1 - \sum_{i=1}^N P(q_k = L_i | \ell_i \hat{\mathbf{p}}_k^+)}{1 - \sum_{i=1}^N P(q_k = L_i | \ell_i \hat{\mathbf{p}}_k^-)}. \end{aligned}$$

Finally, eqns. (36) and (37) are calculated to find the normalized emission probability for all states.

Fig. 3 shows an example of the integral calculations that are required to calculate emission probabilities $b_i(O_k)$ for a road segment with four lanes total, two in each direction,

that are separated by a median. The black dot denotes the estimated position $\hat{\mathbf{p}}_k$ with \hat{f}_k and σ_f^2 denoting the mean and variance in the f -direction of a normal distribution. The lane numbers are indicated along the left edge. The road edges are marked as solid black lines. The lane dividers are marked by dashed black lines. The portion of the probability distribution within each lane is indicated by a distinct color: The blue area accounts for the probability of being in lane L_1 . The green area accounts for the probability of being in lane L_2 . The yellow area accounts for the probability of being in lane L_3 . The red area accounts for the probability of being in lane L_4 . The purple area accounts for the probability of being in L_0 (i.e., not in any lane).

B. Lane Transition Probability Model

The transition probability a_{ij}^k defined in Section II-F is calculated at each time $t_k = kT$ for every lane pair L_i and L_j with $i, j \in 0, \dots, N$.

By the definition of conditional probability, the transition probability defined in eqn. (7) can be rewritten as

$$\begin{aligned} a_{ij}^k &= \frac{P(q_k = L_i, q_{k+1} = L_j, O_k)}{P(q_k = L_i, O_k)} \\ &= \frac{P(q_k = L_i, q_{k+1} = L_j | O_k)P(O_k)}{P(q_k = L_i | O_k)P(O_k)} \\ &= \frac{P(q_k = L_i, q_{k+1} = L_j | O_k)}{P(q_k = L_i | O_k)}. \end{aligned} \quad (46)$$

Eqn. (46) has two probabilities that need to be calculated.

1) *Calculation of $P(q_k = L_i | O_k)$:* The quantity $P(q_k = L_i | O_k)$ represents the probability of being in lane L_i given the estimated position ${}^{\ell}\hat{\mathbf{p}}_k^+$. The probability can be rewritten as

$$P(q_k = L_i | O_k) = P(\mathbf{p}_k \in L_i | {}^{\ell}\hat{\mathbf{p}}_k^+) \quad (47)$$

and calculated using eqn. (42)

2) *Calculation of $P(q_k = L_i, q_{k+1} = L_j | O_k)$:* The quantity $P(q_k = L_i, q_{k+1} = L_j | O_k)$ represents the joint probability of the vehicle being in L_i at time t_k and in L_j at time t_{k+1} given observation O_k . By using the positions $\mathbf{p}_k, \mathbf{p}_{k+1}$, the estimated position $\hat{\mathbf{p}}_k^+$, and the prior predicted position $\hat{\mathbf{p}}_{k+1}^-$, the joint probability can be computed in lane frame as

$$\begin{aligned} P(q_k = L_i, q_{k+1} = L_j | O_k) &= P({}^{\ell}\mathbf{p}_k \in L_i, {}^{\ell}\mathbf{p}_{k+1} \in L_j | O_k) \\ &= P({}^{\ell}\mathbf{p}_k \in L_i, {}^{\ell}\mathbf{p}_{k+1} \in L_j | {}^{\ell}\hat{\mathbf{p}}_k^+, {}^{\ell}\hat{\mathbf{p}}_{k+1}^-). \end{aligned}$$

Within this section let the coordinates of ${}^{\ell}\mathbf{p}_k$ be defined as $[s, f]^\top$ and those of ${}^{\ell}\mathbf{p}_{k+1}$ be denoted as $[s_{k+1}, f_{k+1}]^\top$.

The joint probability requires integration over lane L_i at time t_k and L_j at time t_{k+1}

$$\begin{aligned} &P({}^{\ell}\mathbf{p}_k \in L_i, {}^{\ell}\mathbf{p}_{k+1} \in L_j | O_k) \\ &= \int_{L_j} \int_{L_i} P({}^{\ell}\mathbf{p}_k, {}^{\ell}\mathbf{p}_{k+1} | {}^{\ell}\hat{\mathbf{p}}_k^+, {}^{\ell}\hat{\mathbf{p}}_{k+1}^-) d{}^{\ell}\mathbf{p}_k d{}^{\ell}\mathbf{p}_{k+1} \\ &= \int_{L_j} \int_{L_i} P(s, f, s_{k+1}, f_{k+1} | {}^{\ell}\hat{\mathbf{p}}_k^+, {}^{\ell}\hat{\mathbf{p}}_{k+1}^-) ds df ds_{k+1} df_{k+1}. \end{aligned}$$

Let the coordinates of the estimated vehicle position at time t_{k+1} be defined as ${}^{\ell}\hat{\mathbf{p}}_{k+1}^- = [\hat{s}_{k+1}, \hat{f}_{k+1}]^\top$. The approximation in

eqn. (39) also holds for the integration over both s and s_{k+1} . Thus, the double integral can be simplified as follows with $dD = ds df ds_{k+1} df_{k+1}$

$$\begin{aligned} &\int_{L_j} \int_{L_i} P(s, f, s_{k+1}, f_{k+1} | {}^{\ell}\hat{\mathbf{p}}_k^+, {}^{\ell}\hat{\mathbf{p}}_{k+1}^-) dD \\ &= \int_{L_j} \int_{-\infty}^{\infty} \int_{L_i} \int_{-\infty}^{\infty} P(s, f, s_{k+1}, f_{k+1} | \hat{s}_k, \hat{f}_k, \hat{s}_{k+1}, \hat{f}_{k+1}) dD \\ &= \int_{L_j} \int_{L_i} P(f, f_{k+1} | \hat{f}_k, \hat{f}_{k+1}) df df_{k+1} \\ &= \int_{L_j} \int_{L_i} P(\mathbf{z} | \hat{\mathbf{z}}) d\mathbf{z} \\ &= \int_{L_j} \int_{L_i} \mathbf{A}_{\mathbf{z}} \exp\left(-(\mathbf{z} - \hat{\mathbf{z}})^\top {}^{\ell}\mathbf{C}_{\mathbf{Z}}^{-1} (\mathbf{z} - \hat{\mathbf{z}})\right) d\mathbf{z} \end{aligned} \quad (48)$$

where $\mathbf{A}_{\mathbf{z}} = \frac{1}{2\pi|{}^{\ell}\mathbf{C}_{\mathbf{Z}}|^{\frac{1}{2}}}$, $\mathbf{z} = [f, f_{k+1}]^\top$, $\hat{\mathbf{z}} = [\hat{f}_k, \hat{f}_{k+1}]^\top$, $d\mathbf{z} = df df_{k+1}$, and the error covariance matrix is

$${}^{\ell}\mathbf{C}_{\mathbf{z}} = \begin{bmatrix} \sigma_{f_k}^2 & \rho_{f_k f_{k+1}} \sigma_{f_k} \sigma_{f_{k+1}} \\ \rho_{f_k f_{k+1}} \sigma_{f_k} \sigma_{f_{k+1}} & \sigma_{f_{k+1}}^2 \end{bmatrix}. \quad (49)$$

The various symbols in the definition of ${}^{\ell}\mathbf{C}_{\mathbf{z}}$ of eqn. (49) can be computed from known quantities as follows.

The state vector estimate and its error covariance matrix $\mathbf{C}_{\mathbf{x}_k}$ are defined in Subsection II-D. They are known and can be transformed into any desired reference frame. The standard deviation σ_{f_k} can be extracted from the sub-matrix

$${}^{\ell}\mathbf{C}_{\mathbf{p}_k \mathbf{p}_k} = \begin{bmatrix} \sigma_{s_k}^2 & \rho_{s_k f_k} \sigma_{s_k} \sigma_{f_k} \\ \rho_{s_k f_k} \sigma_{f_k} \sigma_{s_k} & \sigma_{f_k}^2 \end{bmatrix}.$$

The estimated position $\hat{\mathbf{p}}_k$ and prior prediction of the next position $\hat{\mathbf{p}}_{k+1}^-$ are related by

$$\hat{\mathbf{p}}_{k+1}^- = \hat{\mathbf{p}}_k + \hat{\mathbf{v}}_k T. \quad (50)$$

Therefore, the error covariance matrix between $\hat{\mathbf{p}}_k$ and $\hat{\mathbf{p}}_{k+1}^-$ is

$${}^{\ell}\mathbf{C}_{\mathbf{p}_k \mathbf{p}_{k+1}} = {}^{\ell}\mathbf{C}_{\mathbf{p}_k \mathbf{p}_k} + {}^{\ell}\mathbf{C}_{\mathbf{p}_k \mathbf{v}_k} T.$$

The correlation $\rho_{f_k f_{k+1}}$ can be extracted from ${}^{\ell}\mathbf{C}_{\mathbf{p}_k \mathbf{p}_{k+1}}$. Defining $\Phi = [\mathbf{I}, \mathbf{I}T]$, then

$$\begin{aligned} \mathbf{C}_{\mathbf{p}_{k+1} \mathbf{p}_{k+1}} &= \Phi \mathbf{C}_{\mathbf{x}_k} \Phi^\top + \mathbf{Q}_{pp} \\ &= \mathbf{C}_{\mathbf{p}_k \mathbf{p}_k} + 2T \mathbf{C}_{\mathbf{p}_k \mathbf{v}_k} + T^2 \mathbf{C}_{\mathbf{v}_k \mathbf{v}_k} + \mathbf{Q}_{pp} \end{aligned} \quad (51)$$

where \mathbf{Q}_{pp} is the covariance matrix for the process noise. The standard deviation $\sigma_{f_{k+1}}$ can be extracted from $\mathbf{C}_{\mathbf{p}_{k+1} \mathbf{p}_{k+1}}$.

Fig. 4 depicts level curves of the probability ellipses to the position at two subsequent times. The error distribution increases and may rotate during the time advance of eqn. (51).

The joint probability of eqn. (48) can be calculated as

$$\begin{aligned} &P({}^{\ell}\mathbf{p}_k \in L_i, {}^{\ell}\mathbf{p}_{k+1} \in L_j | O_k) \\ &= \int_0^{w_j} \int_0^{w_i} \mathbf{A}_{\mathbf{z}} \exp\left(-(\mathbf{z} - \hat{\mathbf{z}})^\top {}^{\ell}\mathbf{C}_{\mathbf{Z}}^{-1} (\mathbf{z} - \hat{\mathbf{z}})\right) d\mathbf{z}. \end{aligned} \quad (52)$$

Instead of calculating the double integral in eqn. (52), the joint CDF can be used to simplify calculations for each lane pair L_i and L_j . Recall from Section IV, each lane is defined by a sequence of line segments defining the left and right edge of the lane. Using eqn. (33), let \underline{y}_i and \bar{y}_i be the f coordinate

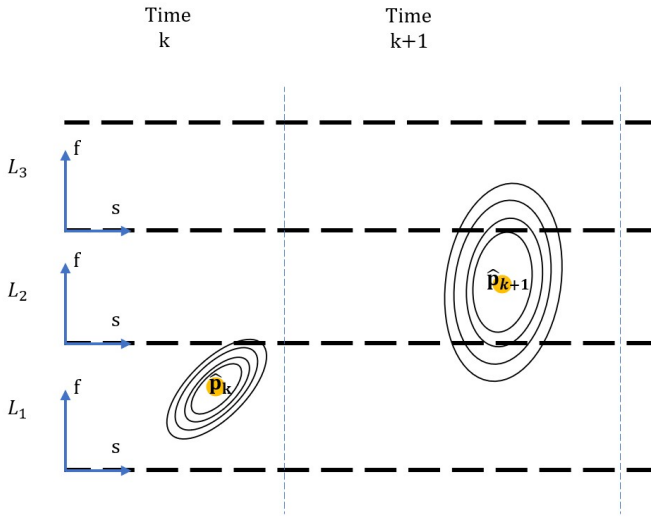


Fig. 4: Probability distribution of the estimated vehicle position at times t_k and t_{k+1} .

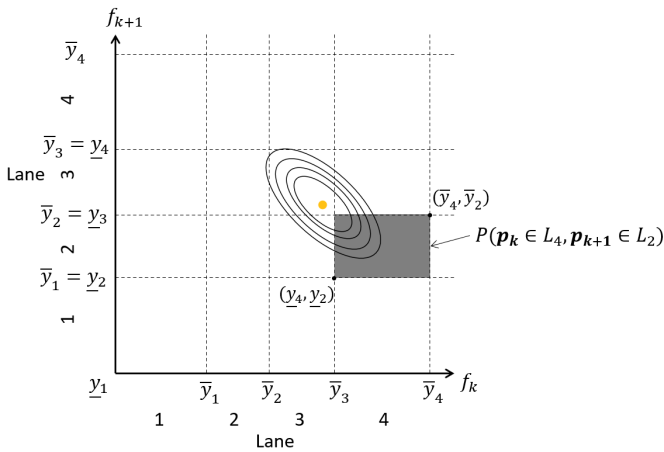


Fig. 5: Calculation of the joint probability of being in lane L_4 at time t_k and lane L_2 at time t_{k+1} , as required for the numerator in Eqn. (46). The ellipse show the contours of constant probability defined by $\hat{\mathbf{z}}$ and ${}^{\ell}\mathbf{C}_z$.

of ${}^{\ell}\mathbf{p}_{v,m}^i$ and ${}^{\ell}\mathbf{p}_{u,m}^i$ respectively, defined in lane frame of L_1 . Then, the joint CDF is defined as

$$P({}^{\ell}\mathbf{p}_k \in L_i, {}^{\ell}\mathbf{p}_{k+1} \in L_j | O_k) = \Phi(\bar{y}_i, \bar{y}_j, \hat{\mathbf{z}}, {}^{\ell}\mathbf{C}_z) - \Phi(\bar{y}_i, \underline{y}_j, \hat{\mathbf{z}}, {}^{\ell}\mathbf{C}_z) - \Phi(\underline{y}_i, \bar{y}_j, \hat{\mathbf{z}}, {}^{\ell}\mathbf{C}_z) + \Phi(\underline{y}_i, \underline{y}_j, \hat{\mathbf{z}}, {}^{\ell}\mathbf{C}_z). \quad (53)$$

The CDF calculation of eqn. (53) is illustrated in Fig. 5. Note that in the figure, all lanes share a lane edge with no median in between. Thus, the following equality holds $\underline{y}_i = \bar{y}_{i-1}$ for $i = 2, 3, 4$.

Each lane at time t_k corresponds to a column of rectangles. Each lane at time t_{k+1} corresponds to a row of rectangles. The height and width of each rectangle match the lane width. The shaded region corresponds to being in lane L_4 at time t_k and lane L_2 at time t_{k+1} . Performing the integration of eqn. (52) or the CDF calculation of eqn. (53) for this shaded region provides the probability of transitioning from lane L_4 at time t_k to lane L_2 at time t_{k+1} .

3) *Calculations of a_{ij}^k Containing Lane L_0 :* Sections V-B1 and V-B2 computed a_{ij}^k for lanes $i, j = 1, \dots, N$ directly. The transition probabilities related to L_0 must be calculated indirectly.

4) *The probability of transitioning to L_0 :* The probability of transitioning to L_0 represents the probability of transitioning to an off road position and is calculated using eqn. (46):

$$a_{i0}^k = \frac{P(q_k = L_i, q_{k+1} = L_0 | O_k)}{P(q_k = L_i | O_k)}.$$

To calculate the numerator, the following property is used

$$\sum_{j=0}^N P(q_k = L_i, q_{k+1} = L_j | O_k) = P(q_k = L_i | O_k).$$

The numerator is calculated as

$$P(q_k = L_i, q_{k+1} = L_0 | O_k) = P(q_k = L_i | O_k) - \sum_{j=1}^N P(q_k = L_i, q_{k+1} = L_j | O_k),$$

where $P(q_k = L_i | O_k)$ is known from eqn. (47) and $P(q_k = L_i, q_{k+1} = L_j | O_k)$ is known from eqn. (53) for $j = 1, \dots, N$. The denominator is calculated using eqn. (42) as discussed in Section V-A.

5) *The probability of transitioning from L_0 :* The probability of transitioning from L_0 represents the probability of transitioning from an off-road position to a lane on the road and is calculated using eqn. (46) as:

$$a_{0j}^k = \frac{P(q_k = L_0, q_{k+1} = L_j | O_k)}{P(q_k = L_0 | O_k)}.$$

The denominator is calculated using eqn. (42) as discussed in Section V-A. To calculate the numerator, the following property is used

$$\sum_{i=0}^N P(q_k = L_i, q_{k+1} = L_j | O_k) = P(q_{k+1} = L_j | O_k).$$

Then the numerator is calculated as

$$P(q_k = L_0, q_{k+1} = L_j | O_k) = P(q_{k+1} = L_j | O_k) - \sum_{i=1}^N P(q_k = L_i, q_{k+1} = L_j | O_k),$$

where $P(q_{k+1} = L_j | O_k)$ is known from eqn. (47) and $P(q_k = L_i, q_{k+1} = L_j | O_k)$ is known from eqn. (53) for $j = 1, \dots, N$.

6) *The probability of transitioning from L_0 to L_0 :* The probability of transitioning from L_0 to L_0 represents the probability of staying off the road and is calculated using the property in eqn. (9) such that

$$a_{00}^k = 1 - \sum_{j=1}^N a_{0j}^k.$$

VI. NON-PARALLEL LANES DETERMINATION AND ROAD SEGMENT SELECTION

The previous sections have only considered the case where all lanes are parallel. This section considers the situation where some lanes are not parallel to the others such as road layouts with merging lanes or highway exits.

As discussed in Section IV, the emission and transition probabilities are calculated in each lane's frame. When the lanes are parallel, the transformations between each lane frame is only a translation of the origin. In that special case, eqns. (42) (45), and (52) can be calculated in the same lane frame.

However, in road layouts where the lanes are not parallel, the emission and transition probability models need to be modified to account for different lane frame orientations and translations.

The emission probability for a non-parallel lane is calculated by eqn. (36). Since the lane frames are not parallel, the probability distribution computation of $P(q_k = L_i | O_k)$ and $P(q_k = L_i)$ will be different in every non-parallel lane frame since the covariance is rotated to that specific frame.

Similarly, the transition probability is modified to account for lane frame orientation changes. Recall from Section V-B that a_{ij}^k has the joint probability $P(q_k = L_i, q_{k+1} = L_j | O_k)$ which needs to be calculated. In order for the joint probability defined in eqn. (52) to work, the covariance ${}^{\ell}\mathbf{C}_z$ needs to be rotated to the proper frame. The rotation matrix ${}^g\mathbf{R}_{im}$ is used to rotate from g-frame to ℓ -frame of lane segment m of lane L_i , defined in Appendix A. The covariance ${}^{\ell}\mathbf{C}_z$ is marginalized from ${}^i\mathbf{C}_{p_k p_k}$, ${}^i\mathbf{C}_{p_k p_{k+1}}$, and ${}^j\mathbf{C}_{p_{k+1} p_{k+1}}$ as described in eqn. (49). Note that ${}^j\mathbf{C}_{p_{k+1} p_{k+1}}$ is rotated to L_j while the rest of the covariances are rotated to L_i using eqn. (58) defined in Appendix A. Similarly, $\hat{\mathbf{p}}_k$ and $\hat{\mathbf{p}}_{k+1}^-$ need to be rotated to L_i and L_j respectively using eqn. (57) defined in Appendix A. Then, the new $\hat{\mathbf{z}} = [\hat{f}_k, \hat{f}_{k+1}]$ and ${}^{\ell}\mathbf{C}_z$ are used to calculate a_{ij}^k using eqn. (52). If there was a need to calculate all variables in the same frame, the mentioned modifications can also be used in parallel lanes without affecting the emission and transition probabilities.

To calculate the HMM probabilities, the lane frame model defined in Section IV uses m to index the road segments. Because the road segment index of the vehicle at each time is not known, the index m has to be calculated.

For each road segment $1 \leq m < M$, let ${}^{\ell}\hat{\mathbf{p}}_k^m = (s_k^m, f_k^m)$ denote the lane coordinates of $\hat{\mathbf{p}}_k$ for the first lane of the segment. The vehicle is on segment m if and only if $s_k^m \geq 0$ and $s_k^{m+1} < 0$.

VII. EXPERIMENT

The goal of this section is to demonstrate and analyze the experimental performance of the HMM and Viterbi methods presented herein in comparison with other methods in the literature.

A. Data Collection Setup and Discussion

To support the experimental analysis GNSS vehicle position and velocity estimates are acquired while a driver performs various lane changes and vehicle maneuvers (e.g., U-turns). Two datasets were collected on Columbia Avenue in Riverside,

California between the intersections with Iowa Avenue and Northgate Street. The driving speed varied from 0 through 45 mph, with typical speeds between 35-45 mph. The driving for data acquisition of a dataset lasted for approximately 32 minutes and included multiple lane changes and U-turns. Throughout the test, the satellite visibility was good (i.e., under open sky conditions).

Two u-blox ZED-F9P dual-frequency receivers were mounted on the vehicle for the experiment. Each was connected to the same u-blox antenna via a signal splitter. The first receiver performs Differential GNSS (DGNSS) using GPS, GALILEO, BeiDou satellites and SBAS corrections. It provides the state estimates that comprise O_k . The second receiver is communicating with a local base station. It uses GPS, GALILEO, and BeiDou satellites to generate its native multi-GNSS, dual frequency, Real-time Kinematic Positioning (RTK)-fixed solution, which uses carrier phase measurements to achieve centimeter-level accuracy [18].

Given this high-level of position accuracy the RTK data was used as the ground truth for the experiment, from which the 'correct' lane sequence could be determined directly. This ground truth lane sequence was used to evaluate correctness of the lane sequences determined by each method based on the data from the first receiver. The RTK data was not otherwise used in any of the results.

To extract \mathbf{C}_{p_k} and \mathbf{C}_{v_k} in g-frame, the receiver binary output was parsed to decode the UBX-NAV-COV protocol, which contains the required covariances. The covariance $\mathbf{C}_{p_k v_k}$ is not part of the UBX-NAV-COV protocol. Because position is computed from pseudorange and velocity is computed from Doppler, herein those measurements are assumed to have independent measurement noise, so that $\mathbf{C}_{p_k v_k}$ was assumed to be a zero matrix.

B. Experiment Datasets

The different lane determination models will be compared using two experiments with two datasets denoted DS 1 and DS 2. DS 1 contains 2045 points while DS 2 contains 1862 points. The data sample rate is one Hertz.

Let ${}^g\mathbf{p}_k = \begin{bmatrix} n_k \\ e_k \end{bmatrix}$ and ${}^g\hat{\mathbf{p}}_k = \begin{bmatrix} \hat{n}_k \\ \hat{e}_k \end{bmatrix}$, the horizontal error at time t_k will be calculated as $e_{h_k} = \sqrt{e_{n_k}^2 + e_{e_k}^2}$ where the north and east errors at time t_k are $e_{n_k} = (\hat{n}_k - n_k)$ and $e_{e_k} = (\hat{e}_k - e_k)$. The mean horizontal error will be calculated as

$$\text{mean error} = \frac{1}{N} \sum_{k=1}^N e_{h_k}.$$

Dataset DS1 has a minimum and maximum horizontal error of 0.03 m and 1.26 m respectively and a mean horizontal error of 0.58 m. Dataset DS2 has a minimum and maximum horizontal error of 0.08 m and 2.55 m respectively and a mean horizontal error of 0.53 m.

DS 1 contains more instances where the vehicle was not in any lane such as when performing a U-turn or entering an intersection. Since the methods that already exist in the literature do not account for off-road positions directly during

the emission and transition probability calculations the comparison will use two experiments:

Experiment 1 uses the two collected datasets. Each dataset includes a complete drive cycle with lane changes and off-road positions. DS 1 contained 192 lane changes, while DS 2 contained 159 lane changes.

Experiment 2 uses a modified version of the two datasets that excludes off-road positions: 199 points are excluded for DS 1, while 61 points are excluded for DS 2.

C. Tested Methods

Five methods will be tested using the experiments and datasets described in Section VII-B:

Proposed Method is the Viterbi approach of Section III using a HMM with the emission and transition probability models defined in Sections V-A and V-B.

Method 2 is the Viterbi approach of Section III using a HMM with the emission probability model proposed in [12] and transition probability model defined in Section V-B.

Method 3 is the Viterbi approach of Section III using a HMM with the emission probability model defined in Section V-A and the transition probability model of [12].

Method 4 is the Viterbi approach of Section III using a HMM with the emission and transition probability models proposed in [12].

Method 5 uses the distance from the estimated vehicle position to the lane center-line as an error function to implement the approach defined in [10], [11]. Let ${}^c\mathbf{p}_k^j$ represent the projection of the estimated position $\hat{\mathbf{p}}_k$ onto the lane center-line of L_j . The error function used the observations \mathcal{O}_{k-d+1}^k at a time t_k , where d is the number of observations used. The error function is

$$err(L_j) = \frac{1}{d} \sum_{i=1}^d \|\ell_i \hat{\mathbf{p}}_{k-d+1} - {}^c\mathbf{p}_{k-d+1}^j\|_2. \quad (54)$$

The sequence of lanes \mathcal{Q}_{k-d+1}^k is set to the one lane L_j which minimizes the error function such that

$$\mathcal{Q}_{k-d+1}^k = \arg \min_{0 \leq j \leq N} err(L_j). \quad (55)$$

The results in [12] were achieved using multiple sensors. Therefore, the emission model in [12] included factors for each sensor modality. That dataset is no longer available. The dataset used herein only includes GNSS data. Therefore, the emission model used herein for Methods 2 and 4 only uses the GNSS observation factor of the emission model in [12].

Methods 3 and 4 both use the transition probability of [12] which does not account for the case of the vehicle not being in a physical lane. When the vehicle is not in a lane (e.g., during a U-turn), these HMM methods may break during the Viterbi algorithm calculations because $\delta_k^+(i) = 0 \forall i$. Herein, we implement a resetting approach referenced by [12], [13] to accommodate these HMM breaks in Methods 2, 3, and 4. When a break is detected, the data is split into separate trips, and the HMM is reinitialized by recalculating eqns. (23) and (24). After the data split, the Viterbi algorithm is run separately

on each trip. The trip paths are then concatenated to generate the complete path. The complete path is then compared to the ground truth to evaluate the accuracy of a given model. At every break, the state at that time step is unknown, and therefore counted as incorrect when evaluating accuracy.

D. Viterbi Algorithm Processing

For each experiment, the Viterbi algorithm summarized in eqns. (23-27) processes observations using three different approaches.

Approach 1 processes the entire sequence of observations \mathcal{O} once at the end of the trip.

Approach 2 processes the most recent five observations \mathcal{O}_{k-4}^k at each t_k with the initialization at each t_{k-4} defined by eqn. (28).

Approach 3 processes the most recent five observations \mathcal{O}_{k-4}^k at each t_k with the initialization at each t_{k-4} defined by eqn. (32).

E. Analysis of the Results

Table IV presents the results from Experiment 1 using the first four methods and both data sets with approximate 95% confidence level. The confidence interval was calculated using the method described in Section 8.1 of [22].

The results for the three approaches are presented in separate sub-tables.

- Proposed Method achieved the highest accuracy in all cases.
- Proposed Method had no breaks. Each of the other methods had several breaks. There are more breaks for DS 1 because it contains more instances where the vehicle was not in any lane. The number of HMM breaks highlights the importance of accounting for off-road locations in lane determination as all methods that do not account for off-road positions in both the emission and transition probabilities suffered from HMM breaks.
- Method 3 used the emission model herein that accounts for off-road positions, while its transition model does not. Such discrepancy affects how the Viterbi algorithm is propagated through time as the maximization in eqn. (25) might not be the optimal solution due to the model's inability to calculate transitions from an off road position, thus lowering the performance.
- Method 4 uses the emission and transition models of [12]. Changing only the transition model of [12] to that proposed herein (i.e., Method 2) yielded an average accuracy increase of 1.8% and 2.8% for Datasets 1 and 2.

Table V presents the results from Experiment 2 (excluding off-road positions) using the first four methods and both datasets. The results for each approach are presented in a separate sub-tables.

- In Approaches 1 and 3, Proposed Method, Method 2, and Method 4 achieve similar levels of accuracy with Method 2 achieving the highest accuracy within margin of error of the Proposed Method.

| Approach 1 | | | | |
|-----------------|------------------------------------|------------------|------------------------------------|------------------|
| | Accuracy | Number of Breaks | Accuracy | Number of Breaks |
| Proposed Method | 95.6% \pm 0.9% | 0 | 95.1% \pm 1.0% | 0 |
| Method 2 | 88.4% \pm 1.4% | 144 | 93.9% \pm 1.1% | 20 |
| Method 3 | 61.2% \pm 2.1% | 172 | 74.6% \pm 2.0% | 42 |
| Method 4 | 84.6% \pm 1.6% | 170 | 89.6% \pm 1.4% | 43 |
| Approach 2 | | | | |
| | Accuracy | Number of Breaks | Accuracy | Number of Breaks |
| Proposed Method | 96.0% \pm 0.9% | 0 | 95.0% \pm 1.0% | 0 |
| Method 2 | 88.3% \pm 1.4% | 139 | 93.9% \pm 1.1% | 16 |
| Method 3 | 71.2% \pm 2.0% | 172 | 77.9% \pm 1.9% | 20 |
| Method 4 | 86.9% \pm 1.5% | 175 | 92.2% \pm 1.2% | 41 |
| Approach 3 | | | | |
| | Accuracy | Number of Breaks | Accuracy | Number of Breaks |
| Proposed Method | 96.3% \pm 0.8% | 0 | 95.1% \pm 1.0% | 0 |
| Method 2 | 88.3% \pm 1.4% | 140 | 93.9% \pm 1.1% | 16 |
| Method 3 | 69.2% \pm 2.0% | 297 | 70.7% \pm 2.1% | 136 |
| Method 4 | 86.2% \pm 1.5% | 301 | 91.5% \pm 1.3% | 146 |

TABLE IV: Experiment 1 results. Columns 2 and 3 present the results using DS 1, while columns 4 and 5 present the results using DS 2.

| Approach 1 | | | | |
|-----------------|------------------------------------|------------------|------------------------------------|------------------|
| | Accuracy | Number of Breaks | Accuracy | Number of Breaks |
| Proposed Method | 96.9% \pm 0.8% | 0 | 95.8% \pm 0.9% | 0 |
| Method 2 | 97.6% \pm 0.7% | 8 | 96.4% \pm 0.9% | 3 |
| Method 3 | 65.3% \pm 2.2% | 36 | 76.6% \pm 2.0% | 26 |
| Method 4 | 95.4% \pm 1.0% | 33 | 94.7% \pm 1.0% | 27 |
| Approach 2 | | | | |
| | Accuracy | Number of Breaks | Accuracy | Number of Breaks |
| Proposed Method | 97.0% \pm 0.8% | 0 | 95.7% \pm 0.9% | 0 |
| Method 2 | 88.3% \pm 1.5% | 6 | 93.5% \pm 1.1% | 0 |
| Method 3 | 66.1% \pm 2.2% | 36 | 76.5% \pm 2.0% | 11 |
| Method 4 | 86.9% \pm 1.5% | 47 | 91.9% \pm 1.3% | 34 |
| Approach 3 | | | | |
| | Accuracy | Number of Breaks | Accuracy | Number of Breaks |
| Proposed Method | 96.9% \pm 0.8% | 0 | 95.7% \pm 0.9% | 0 |
| Method 2 | 97.8% \pm 0.7% | 9 | 96.7% \pm 0.8% | 0 |
| Method 3 | 70.6% \pm 2.1% | 146 | 72.2% \pm 2.1% | 120 |
| Method 4 | 95.5% \pm 0.9% | 160 | 94.3% \pm 1.1% | 130 |

TABLE V: Experiment 2 results using a parsed version of DS 1 and DS2, where off road positions are excluded. The columns have the same interpretations as Table IV.

- In Approach 2, Proposed Method achieves the best accuracy by approximately 10%.
- Proposed Method experiences no breaks, whereas all of the other Methods still experience breaks even though all off-road positions have been excluded. This suggests that HMM breaks are still possible based on the emission and transition probability model combinations used in Methods 2-4 and are not only caused by off-road positions.
- Method 4 uses the emission and transition models of [12]. Changing only the transition model of [12] to that proposed herein (i.e., Method 2) yielded an average accuracy increase of 1.9% for both Datasets 1 and 2.

Since Method 5 does not use the Viterbi algorithm, its results are reported separately. Table VI presents the results of using Method 5 for both datasets, using three different values of its parameter d : 1, 3, and 5. At each time instant, Method 5 selects the road segment as described in Section VI. When

| Experiment 1 Results | | |
|----------------------|--------------------------------------|--------------------------------------|
| Observations used | DS 1 Accuracy | DS 2 Accuracy |
| $d = 1$ | $89.0\% \pm 1.4\%$ | $94.5\% \pm 1.0\%$ |
| $d = 3$ | $85.4\% \pm 1.5\%$ | $91.1\% \pm 1.3\%$ |
| $d = 5$ | $81.1\% \pm 1.7\%$ | $87.5\% \pm 1.5\%$ |

| Experiment 2 Results | | |
|----------------------|--------------------------------------|--------------------------------------|
| Observations used | DS 1 Accuracy | DS 2 Accuracy |
| $d = 1$ | $98.6\% \pm 0.5\%$ | $97.7\% \pm 0.7\%$ |
| $d = 3$ | $92.7\% \pm 1.2\%$ | $94.6\% \pm 1.0\%$ |
| $d = 5$ | $88.8\% \pm 1.4\%$ | $89.7\% \pm 1.4\%$ |

TABLE VI: Method 5 results.

the vehicle is not on the road, Method 5 will still report a closest lane; herein these instances are counted as incorrect for evaluating accuracy in the tabulation of results. Method 5 is able to achieve high accuracy in Experiment 2, when all off-road positions are removed. Method 5 is also able to produce the highest accuracy with $d = 1$ in Experiment 2; however, because it only utilizes the estimated position at a single time to calculate the most probable lane, Method 5 will be the method most negatively affected by GNSS inaccuracies, which explains why it is not consistently the best performing method.

VIII. CONCLUSION

This paper introduced a new lane determination approach that determines the data-dependent HMM emission and transition model parameters by processing navigation system data relative to the road/lane geometry. This method achieves enhanced reliability and accuracy because it accounts for the continuously changing probabilities as the vehicle travels along the road. Two versions of a real-time Viterbi algorithm variation are also proposed as alternatives that have fixed computational requirements.

A. Experimental Results

The experiment results show that the data-dependent HMM approach that relies on the lane geometry and vehicle state estimates, to calculate the HMM transition and emission probabilities, provides an increase in accuracy and reliability compared to existing lane determination methods in the literature. Moreover, the proposed model does not require any training or parameter tuning, which improves generality. The proposed model also provides a method of dealing with situations where the vehicle is not in a lane by introducing a no lane state with its own emission and transition probabilities. Thus, removing the need for post-processing and removal of observations to deal with possible HMM breaks.

B. Future Work

The proposed model has only been tested using GNSS data to generate the set of observations \mathcal{O} . Future work could explore including additional sensor and vehicle information. These modifications will require an extension to the data-dependent HMM, after which, the Viterbi Algorithm performance should improve further.

IX. ACKNOWLEDGMENT

This work was partially funded by support from the U.S. Department of Energy EcoCAR EV Challenge, a gift from Mitsubishi Electric Research Laboratories (MERL), the National Center for Sustainable Transportation (NCST), and the UCR KA Endowment.

APPENDIX

The following appendix describes concepts important to the paper that are too detailed for the main body.

A. Frame Definitions

Throughout the paper, the vehicle state vector $\mathbf{X}_k = [\mathbf{p}_k, \mathbf{v}_k]^\top$ is represented in various frames-of-reference where \mathbf{p}_k and \mathbf{v}_k represent the position and velocity of the vehicle. The three frames used in the paper consist of ECEF (e), intersection (g), and lane (ℓ) frame-of-reference.

ECEF Frame (e) Every T seconds, the GNSS receiver provides position measurements ${}^e\tilde{\mathbf{p}} \in \mathbb{R}^3$ in ECEF frame. The paper only utilizes Cartesian coordinates because it facilitates vector mathematics and simplifications. If a sensor or device communicates geodetic coordinates, the measurements will be converted to the equivalent Cartesian coordinates using the methods in Section 2.3.3 of [23].

Intersection Frame (g) The origin of the intersection frame (g) is located at the point \mathbf{T}_{eg} with ECEF coordinates ${}^e\mathbf{T}_{eg}$, which are known. The axes of g-frame point in the north, east, and down directions.

The transformation of ECEF Cartesian coordinates ${}^e\mathbf{p}$ from e-frame to g-frame is described in Section 2.4.2 of [23] as:

$${}^g\mathbf{p} = {}_e^g\mathbf{R} ({}^e\mathbf{p} - {}^e\mathbf{T}_{eg}), \quad (56)$$

where the matrix ${}_e^g\mathbf{R}$ rotates vectors from the e-frame to g-frame. The rotation matrix ${}_e^g\mathbf{R}$ is computed based on the origin ${}^e\mathbf{T}_{eg}$, as discussed in Section 2.5.2 of [23].

Lane Frame (ℓ) For lane segment m of lane i , the origin is at the location with geodetic coordinates ${}^g\mathbf{p}_{(v,m)}^i$.

The transformation of the g-frame position ${}^g\mathbf{p}$ to ℓ -frame for lane segment m of the i -th lane is

$${}^{\ell}\mathbf{p} = {}_g^{\ell}\mathbf{R}_{im} ({}^g\mathbf{p} - {}^g\mathbf{p}_{(v,m)}^i), \quad (57)$$

where the rotation matrix ${}_g^{\ell}\mathbf{R}_{im}$ is defined as

$${}_g^{\ell}\mathbf{R}_{im} = \begin{bmatrix} \cos \alpha & -\sin \alpha \\ \sin \alpha & \cos \alpha \end{bmatrix}.$$

The angle α is defined as the rotation around the down vector to align the geodetic e-axis with the lane s-axis.

When a covariance matrix is known in one frame and needed in another, it can be computed using the rotation matrix. For example, if ${}^g\mathbf{C}_{\mathbf{p}_k}$ is available and ${}^{\ell}\mathbf{C}_{\mathbf{p}_k}$ is required

$${}^{\ell}\mathbf{C}_{\mathbf{p}_k} = {}_g^{\ell}\mathbf{R}_{im} {}^g\mathbf{C}_{\mathbf{p}_k} {}_g^{\ell}\mathbf{R}_{im}^\top. \quad (58)$$

REFERENCES

- [1] J. Farrell, G. Wu, W. Hu, D. Oswald, and P. Hao, "Lane-Level Localization and Map Matching for Advanced Connected and Automated Vehicle (CAV) Applications," *UC Davis: National Center for Sustainable Transportation*, 2023. [Online]. Available: <https://doi.org/10.7922/G25T3HSS>
- [2] O. D. Altan, G. Wu, M. J. Barth, K. Boriboonsomsin, and J. A. Stark, "GlidePath: Eco-friendly automated approach and departure at signalized intersections," *IEEE Transactions on Intelligent Vehicles*, vol. 2, no. 4, pp. 266–277, 2017.
- [3] W. Hu, D. Oswald, G. Wu, and J. A. Farrell, "Assessment of US Department of Transportation Lane-Level Map for Connected Vehicle Applications," *arXiv preprint arXiv:2206.13774*, 2022.
- [4] J. Du, J. Masters, and M. Barth, "Lane-level Positioning for In-Vehicle Navigation and Automated Vehicle Location (AVL) Systems," in *Proceedings. The 7th International IEEE Conference on Intelligent Transportation Systems (IEEE Cat. No. 04TH8749)*. IEEE, 2004, pp. 35–40.
- [5] J. Du and M. J. Barth, "Next-Generation Automated Vehicle Location Systems: Positioning at The Lane Level," *IEEE Transactions on Intelligent Transportation Systems*, vol. 9, no. 1, pp. 48–57, 2008.
- [6] J. Rabe, M. Meinke, M. Necker, and C. Stiller, "Lane-level Map-Matching Based on Optimization," in *2016 IEEE 19th International Conference on Intelligent Transportation Systems (ITSC)*. IEEE, 2016, pp. 1155–1160.
- [7] F. Li, P. Bonnifait, J. Ibanez-Guzman, and C. Zinoune, "Lane-level map-matching with integrity on high-definition maps," in *2017 IEEE Intelligent Vehicles Symposium (IV)*. IEEE, 2017, pp. 1176–1181.
- [8] C. Goh, J. Dauwels, N. Mitrovic, M. T. Asif, A. Oran, and P. Jaillet, "Online map-matching based on Hidden Markov Model for Real-Time Traffic Sensing Applications," in *2012 15th International IEEE Conference on Intelligent Transportation Systems*, 2012, pp. 776–781.
- [9] Y. Hu and B. Lu, "A Hidden Markov Model-Based Map Matching Algorithm for Low Sampling Rate Trajectory Data," *IEEE Access*, vol. 7, pp. 178 235–178 245, 2019.
- [10] M. M. Atia, A. R. Hilal, C. Stellings, E. Hartwell, J. Toonstra, W. B. Miners, and O. A. Basir, "A Low-Cost Lane-Determination System Using GNSS/IMU Fusion and HMM-Based Multistage Map Matching," *IEEE Transactions on Intelligent Transportation Systems*, vol. 18, no. 11, pp. 3027–3037, 2017.
- [11] S. Fu, W. Chen, H. Kong, H. Zheng, L. Du, and C. Li, "Lane-Level Map-Matching at Multilane Intersections Based on Network RTK and Internet of Vehicle," in *2019 5th International Conference on Transportation Information and Safety (ICTIS)*, 2019, pp. 718–722.
- [12] A. Hansson, E. Korsberg, R. Maghsoud, E. Nordén, and Selpi, "Lane-Level Map Matching Based on HMM," *IEEE Transactions on Intelligent Vehicles*, vol. 6, no. 3, pp. 430–439, 2021.
- [13] P. Newson and J. Krumm, "Hidden Markov Map Matching Through Noise and Sparseness," in *Proceedings of the 17th ACM SIGSPATIAL International Conference on Advances in Geographic Information Systems*, ser. GIS '09. New York, NY, USA: Association for Computing Machinery, 2009, p. 336–343. [Online]. Available: <https://doi.org/10.1145/1653771.1653818>
- [14] D. Jurafsky and J. H. Martin. (2023) Speech and language processing. [Online]. Available: <https://web.stanford.edu/~jurafsky/slp3/A.pdf>
- [15] L. Rabiner, "A tutorial on hidden markov models and selected applications in speech recognition," *Proceedings of the IEEE*, vol. 77, no. 2, pp. 257–286, 1989.
- [16] P. S. Maybeck, *Stochastic Models, Estimation, and Control*, ser. Mathematics in Science and Engineering : a series of monographs and textbooks. Academic Press, 1979, vol. 1.
- [17] B. Hofmann-Wellenhof, H. Lichtenegger, and E. Wasle, *GNSS-global navigation satellite systems: GPS, GLONASS, Galileo, and more*. Springer Science & Business Media, 2007.
- [18] P. Teunissen and O. Montenbruck, *Springer Handbook of Global Navigation Satellite Systems*. Springer, 2017.
- [19] W. Hu, A. Neupane, and J. A. Farrell, "Using PPP Information to Implement a Global Real-Time Virtual Network DGNSS Approach," *IEEE Transactions on Vehicular Technology*, vol. 71, no. 10, pp. 10 337–10 349, 2022.
- [20] J. Kreibich, F. Brenner, and M. Lienkamp, "Lane-Level Matching Algorithm Based on GNSS, IMU and Map Data," in *2021 8th International Conference on Soft Computing & Machine Intelligence (ISCFMI)*. IEEE, 2021, pp. 211–218.

- [21] F. Rahman, F. O. Silva, Z. Jiang, and J. A. Farrell, "Low-Cost Real-Time PPP GNSS Aided INS for CAV Applications," *IEEE Transactions on Intelligent Transportation Systems*, vol. 23, no. 12, pp. 25 018–25 032, 2022.
- [22] D. S. Moore, G. P. McCabe, and B. A. Craig, *Introduction to the Practice of Statistics*, 6th ed. W. H. Freeman and Company, 2009.
- [23] J. A. Farrell, *Aided Navigation: GPS with High Rate Sensors*. McGraw-Hill, Inc., 2008.

ACRONYMS

- CAV** Connected and Automated Vehicle
- CDF** Cumulative Distribution Function
- DGNSS** Differential GNSS
- ECEF** Earth-Centered Earth-Fixed
- GNSS** Global Navigation Satellite System
- HMM** Hidden Markov Model
- INS** Inertial Navigation System
- ITS** Intelligent Transportation Systems
- NED** North, East, and Down
- RTK** Real-time Kinematic Positioning
- V2X** Vehicle-to-Everything

Mike Stas received the B.S and M.S degrees in electrical engineering from University of California, Riverside. He is pursuing his Ph.D degree in Electrical Engineering at the University of California, Riverside, USA. His research interests include Connected and Automated Vehicle (CAV) systems, GNSS, GNSS spoofing detection and its effects on CAV systems, aided inertial navigation, and state estimation.

Wang Hu received the B.Eng. degree in electronics and information engineering from North China Electric Power University, Beijing, China. He is pursuing his Ph.D. degree in Electrical and Computer Engineering at the University of California, Riverside, CA, USA. His research interests include automated driving, GNSS, aided inertial navigation, and state estimation.

Jay Farrell is the KA Endowed Professor of ECE at the University of California, Riverside. He has served as General Chair of the 2012 IEEE Conference on Decision and Control, President of the IEEE CSS, and President of the American Automatic Control Council. At Draper Lab, Farrell received the Engineering VP's Best Technical Publication Award in 1990, and Recognition Awards for Outstanding Performance and Achievement in 1991 and 1993. He is a Fellow of the IEEE, AAAS, and IFAC and author of 3 books and over 250 technical publications.